ISSN (Print) 1226-1750
ISSN (Online) 2233-6656
Journal of Magnetics 22(1), 34-42 (2017) https://doi.org/10.4283/JMAG.2017.22.1.034

Magnetic Flux Leakage (MFL) based Defect Characterization of Steam Generator Tubes using Artificial Neural Networks

Jackson Daniel[1]*, A. Abudhahir[2], and J. Janet Paulin[1]

[1]*National Engineering College, Department of Electronics and Instrumentation Engineering, Kovilpatti, Tamilnadu, India*
[2]*Vel Tech Multitech Dr. Rangarajan Dr. Sakunthala Engineering College, Department of Electrical and Electronics Engineering, Chennai, India*

(Received 18 August 2016, Received in final form 26 December 2016, Accepted 4 January 2017)

Material defects in the Steam Generator Tubes (SGT) of sodium cooled fast breeder reactor (PFBR) can lead to leakage of water into sodium. The water and sodium reaction will lead to major accidents. Therefore, the examination of steam generator tubes for the early detection of defects is an important requirement for safety and economic considerations. In this work, the Magnetic Flux Leakage (MFL) based Non Destructive Testing (NDT) technique is used to perform the defect detection process. The rectangular notch defects on the outer surface of steam generator tubes are modeled using COMSOL multiphysics 4.3a software. The obtained MFL images are de-noised to improve the integrity of flaw related information. Grey Level Co-occurrence Matrix (GLCM) features are extracted from MFL images and taken as input parameter to train the neural network. A comparative study on characterization have been carried out using feed-forward back propagation (FFBP) and cascade-forward back propagation (CFBP) algorithms. The results of both algorithms are evaluated with Mean Square Error (MSE) as a prediction performance measure. The average percentage error for length, depth and width are also computed. The result shows that the feed-forward back propagation network model performs better in characterizing the defects.

Keywords : Magnetic Flux Leakage (MFL), Gray Level Co-occurence Matrix (GLCM), Neural Network (NN), cascade-forward back propagation (CFBP), feed-forward back propagation (FFBP)

1. Introduction

Non Destructive Testing techniques are currently prevailing among the most widespread techniques for the rapid inspection of steam generator tube in the nuclear power industry [1]. The steam generator tube is continuously exposed to severe environmental conditions such as high fluid flow rate, high temperatures and high pressures [2]. Critical components such as Steam Generator Tubes (SGT), feed water heaters, and pressure vessels have rigorous design requirements regarding their structural integrity. To improve the safety and reliability of an industry, continuous monitoring of the structural integrity of these equipments is very essential. Therefore, some non destructive testing techniques have been developed and applied for structural defect inspection during manufacture and regular maintenance. The techniques include electromagnetic testing, ultrasonic testing, and others. These methods are quite effective and accurate in detecting structural flaws in steam generator tubes and steam pipes [3]. Eddy current technique is a surface inspection method. It has the limitation to size the flaw accurately because the eddy current measures the impedance represented by the conductivity change associated with the volumetric change of flaws, where the permeability of flaw is considered unity. The evaluation of small defect is limited in remote field eddy current technique. Wall loss detectability is limited to 20 % or greater. The major advantage of MFL inspection over other nondestructive techniques is that it can detect corrosion and other defects not only on the surface of the tube but also on the opposite side as well. The steam generator tubes which is made of ferromagnetic material are periodically inspected for cracks, notches and corrosion type defects using magnetic flux leakage methods [4]. The MFL method is a fast and reliable NDT technique that has been widely used for decades. When the test object is uniformly magnetised and if any defect presents in the test object due to reduc-

*Corresponding author: Tel: +91-94424-45330
Fax: +91-4632-232749, e-mail: jdeie@nec.edu.in

tion in magnetic permeability, the magnetic flux lines leak out of the object around the defect. The changeable fields are captured by Hall-effect probes, placed directly above the surface of the testing tube which generate signals can be used to recognize the defects [5]. Like in other non destructive testing techniques, solution of the inverse problem of predicting the size of defects from measured magnetic flux leakage signals is of ultimate interest in the community [6]. Certain methods detect the flux leakage from the cracks in ferromagnetic material which is magnetized by an electromagnet [7]. The simulated MFL images are also used in order to characterize the defect present in it. Automatic measurement system has already been developed for detecting the backside defects of large structures [8]. The depth estimation from the magnetic flux leakage signals of complex defects on the underground gas pipelines are analyzed. The average depth error of 8.59 % and width error of 15.55 % and average length error of 5.8 % has already been reported [9]. The problem of defect detection and sizing has been addressed by many researchers in the literature [10-16]. The use of neural networks for pattern recognition of MFL signals and classification of three types of defects in the weld joint has already been reported in the literature. The results shown that it is possible to classify signals of classes of defect and non-defect using NN with 94.2 % efficiency. Moreover, the algorithm is possible to classify the defect pattern signals using neural networks with an average rate of success of 71.7 % for the validation set [17]. Estimation of length and width of the metal-loss profiles from the 1-D signal of the defects has been carried out. Even though the result shows the match with actual size and shape of defects, the quantitative evaluations of defects are not addressed [18]. In most of the literature, while characterizing the defects, the classifications of different types of defects have been performed instead of sizing the defects. Though few works have been documented related to quantitative characterization of the defects, the accuracy imposed is not up to the greatest level in evaluating the surface defects of steam generator tube with the outer diameter of 12.6 mm. In this paper, the magnetic flux leakage images of the defect in steam generator tube have been obtained by modeling the MFL inspection system using COMSOL 4.3a software. Twenty two features including fourteen Haralick features from the Gray Level Co-occurrence Matrix are extracted for each image. GLCM represents the distributions of the intensities and the information about the relative positions of neighboring pixels of an image [19]. The extracted twenty two haralick features have been used as the input parameters for neural network training. The actual defect size such as length, width and depth have been given as target. A performance comparison of FFBP and CFBP network for characterizing the defects in MFL images have been made.

2. Proposed Method

The Characterization of outer surface rectangular defect in a steam generator tube has been performed to measure the length, width and depth of the defects. The defective Magnetic Flux Leakage image has been obtained by modeling the MFL imaging system using COMSOL 4.3a Multiphysics modeling software. The detailed sequence of the proposed defect characterization algorithm is shown in Fig. 1. The radial defect present in the outer surface of steam generator tube is considered in this work. The magnetizing probe and hall sensor arrangements are placed inside the steam generator tube which is of 100 mm length, 17.4 mm outer diameter and 2.3 mm wall thickness. After the pre-processing, feature extraction from GLCM of MFL images and defect characterization using training and testing of artificial neural networks have been performed using Matlab Software. An error-back propagation learning algorithm is used in this feed-forward and

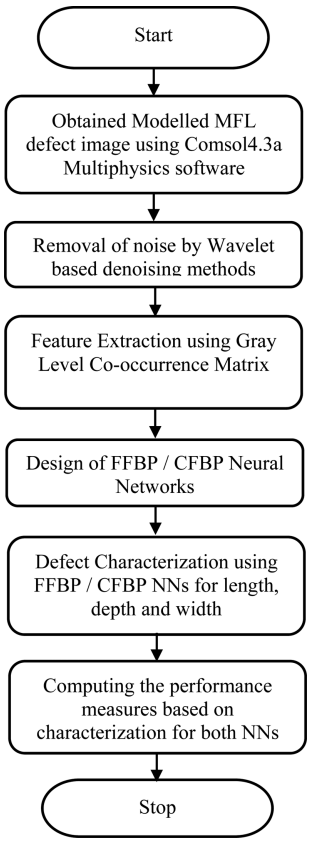

Fig. 1. Flow chart for the proposed defect characterization algorithm.

cascade-forward neural networks in order to train the input feature set.

2.1. Magnetic Flux Leakage (MFL) Imaging

The finite element modeling of MFL system has been obtained through COMSOL 4.3a software. 3D view of the modeled MFL system along with the magnetizing arrangement are shown in Fig. 2(a). The model employs a steel bobbin with 50 mm length, 11.3 mm Outer diameter at the edges and 2.5 mm at the centre. A multi turn copper coil is wound over the bobbin coil to magnetize the SG tube. A strip of 64 Hall sensors called cutline sensor is placed inside the tube and circumferentially arranged over the bobbin coil. The dimension of bobbin coil arrangement is shown in Fig. 2(b). Linear scanning is performed with the above said arrangement to obtain the leakage signal for the length of 50 mm of the tube [20]. This is further changed into a gray scale image in defect characterization process. 64 hall sensors with equal spacing are positioned over the circumference of the bobbin coil at the inner side of the SGT. 51 scanning movements are given linearly and the data obtained is 64 × 51. SGT of 100 mm length is taken for this work and the data obtained is only for the length of 50 mm which is considered for further analysis. Figure 3 shows the gray scale image of the steam generator tube with outer surface defects.

Numerous reasons exist that can contaminate the MFL signal congregated from a pipeline. These major reasons include variations in the position of the sensors (lift-off)

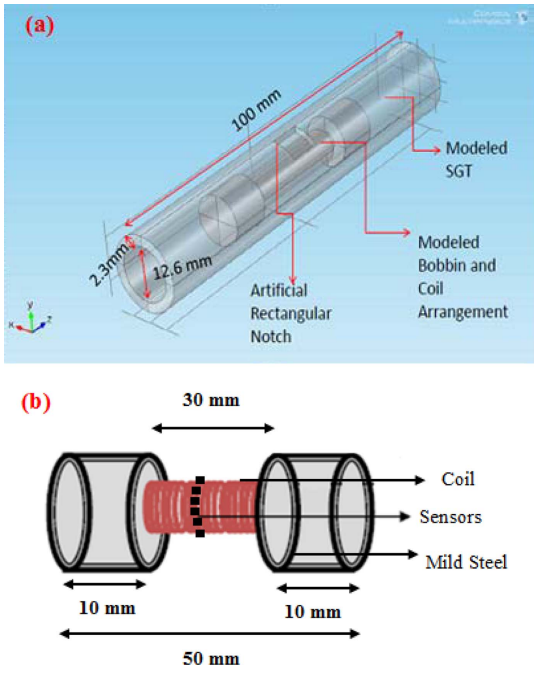

Fig. 2. (Color online) (a) 3D geometry of tube and bobbin coil arrangement (b) dimension of the bobbin coil.

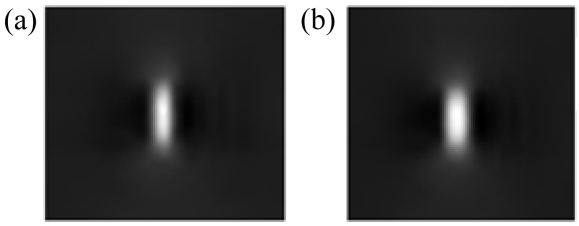

Fig. 3. MFL images of SGT with surface defects (a) length 2 mm, depth 1.15 mm, width 13.5 mm (b) length 3 mm, depth 1.38 mm, width 13.5 mm.

and pipe noise due to the grain structure of pipe material [21]. Daniel *et al.* performed denoising methods for MFL images in order to choose the best wavelet family in denoising MFL images, four wavelet de-noising techniques such as Haar, db4, db8 and symlet have been performed to remove noise from the raw data. The performance measures are evaluated [22]. Based on performance measures, Debauchies 4 wavelet de-noising technique is used for filtering the MFL images.

2.2. GLCM feature extraction

Texture is an important feature used to identify the region of interest in an image. In general 14 Haralic features in the GLCM provide fundamental significant characteristics in identifying the region in an image. But the haralic texture feature is the first order statistical feature and it does not contain the neighbourhood pixel information. For defect segmentation, classification and characterization, the neighbourhood pixel information is very much useful in discriminating the object. The features other than haralick in the grey level occurrence matrix (GLCM) represent the neighbourhood pixel information which represents second order statistical features. co-occurrence matrix of the statistical approach provides valuable information about the relative position of the neighbouring pixels in an image. Hence twenty two features are extracted from the image. So, each element (i, j) of the matrix is the number of occurrences of the pair of pixel with value i and a pixel with value j which are at a distance d relative to each other [23, 24].

For a given MFL image I of size $N \times N$, the elements of a $G \times G$ gray-level co-occurrence matrix M_{co} for a displacement vector $d = (dx, dy)$ is defined mathematically as shown in Eq. (1)

$$M_{co} = \sum_{x=1}^{N}\sum_{y=1}^{N}\begin{Bmatrix}1, if\ I(x,y) = i\ and\ I(x+d_x, y+d_y) = j\\ 0, otherwise\end{Bmatrix} \quad (1)$$

Following representations are used to obtain the various GLCM features with distance $d = 1$ and angle at 0°. Various literature studies show the d values ranging from 1 to 10.

By choosing higher values for *d*, results gets lost in neibourhood pixel feature which leads to poor classification. *G* is the number of different gray levels in an image. μ_x and μ_y are the means of P_x and P_y. σ_x and σ_y are standard deviations of P_x and P_y. $P_x(i)$ is the i[th] entry in the matrix which is obtained by summing the rows of $P(i, j)$. The expressions for GLCM, mean and standard deviations are depicted from the equation (2) to the equation (12).

$$P_x(i) = \sum_{j=0}^{G-1} p(i,j) \tag{2}$$

$$P_y(i) = \sum_{i=0}^{G-1} p(i,j) \tag{3}$$

$$\mu = \sum_{i,j=0}^{G-1} i\, p(i,j) \tag{4}$$

$$\mu = \sum_{i=0}^{G-1} i \sum_{j=0}^{G-1} p(i,j) = \sum_{i=0}^{G-1} i\, P_x(i) \tag{5}$$

$$\mu_y = \sum_{i=0}^{G-1} i \sum_{j=0}^{G-1} j\, p(i,j) = \sum_{i=0}^{G-1} j\, P_y(j) \tag{6}$$

$$\sigma_x^{\,2} = \sum_{i=0}^{G-1} (i-\mu_x)^2 \sum_{j=0}^{G-1} p(i,j) = \sum_{i-0}^{G-1} (P_x(i) - \mu_x(i))^2 \tag{7}$$

$$\sigma_y^{\,2} = \sum_{i=0}^{G-1} (j-\mu_y)^2 \sum_{j=0}^{G-1} p(i,j) = \sum_{i-0}^{G-1} (P_x(i) - \mu_x(i))^2 \tag{8}$$

$$p_{(x+y)}(K) = \sum_{i=0}^{G-1} \sum_{j=0}^{G-1} P(i,j) \text{ for } k = 0, 1 \ldots\ldots, 2(G-1) \tag{9}$$

$$HXY = \sum_{i,j=0}^{G-1} P(i,j) \log_2 P(i,j) \tag{10}$$

$$HXY1 = \sum_{i,j=0}^{G-1} P(i,j) \log_2 (P_x(i) P_y(i)) \tag{11}$$

$$HXY2 = \sum_{i,j=0}^{G-1} (P_x(i) P_y(i) \log_2 (P_x(i) P_y(i)) \tag{12}$$

The Expressions of 22 Gray Level Co-occurrence features are given by the equation (13) to (34)

$$\text{Energy/Uniformity (UNF)} = \sum_{i=0}^{G-1} \sum_{j=0}^{G-1} P(i,j)^2 \tag{13}$$

$$\text{Entropy (ETR)} = \sum_{i=0}^{G-1} \sum_{j=0}^{G-1} P(i,j) \log(P(i,j)) \tag{14}$$

$$\text{Dissimilarity (DSL)} = \sum_{i=0}^{G-1} \sum_{j=0}^{G-1} |i-j|\, P(i,j) \tag{15}$$

$$\text{Contrast (CST)} = \sum_{i=0}^{G-1} \sum_{j=0}^{G-1} P(i,j)(i-j)^2 \tag{16}$$

$$\text{Inverse Difference (ID)} = \sum_{i=0}^{G-1} \sum_{j=1}^{G-1} \frac{p_{ij}}{1+(i-j)} \tag{17}$$

$$\text{Correlation (CN)} = \sum_{i=0}^{G-1} \sum_{j=1}^{G-1} p(i,j) X(i\, X\, j) - (\mu_x\ \mathrm{X}\ \mu_y) / \sigma_x \sigma_y \tag{18}$$

$$\text{Homogeneity (H)} = \sum_{i=0}^{G-1} \sum_{j=0}^{G-1} \frac{p_{(i,j)}}{1+|i-j|} \tag{19}$$

$$\text{Auto correlation (AC)} = \sum_{i=0}^{G-1} \sum_{j=1}^{G-1} (p_x - \mu_x)\,(p_y - \mu_y) / \sigma_x \sigma_y \tag{20}$$

$$\text{Cluster shade (CS)} = \sum_{i=0}^{G-1} \sum_{j=1}^{G-1} P(i,j)\,(i+j-\mu_x-\mu_y)^3 \tag{21}$$

$$\text{Cluster prominence (CP)} = \sum_{i=0}^{G-1} \sum_{j=0}^{G-1} P(i,j)\,(i+j-\mu_x-\mu_y)^4 \tag{22}$$

$$\text{Maximum Probability (MP)} = \max(i,j)\, P(i,j) \tag{23}$$

$$\text{Sum of squares: variance (SS)} = \sum_{i=0}^{G-1} \sum_{j=0}^{G-1} P(i,j)\,(i-\mu)^2 \tag{24}$$

$$\text{Sum average (SA)} = \sum_{i=0}^{2G-2} i\, P_{x+y}(i) \tag{25}$$

$$\text{Sum Variance (SV)} = \sum_{i=0}^{2G-2} (i-s\alpha)^2\, P_{x+y}(i) \tag{26}$$

$$\text{Sum entropy (SE)} = -\sum_{i=0}^{2G-2} P_{x+y}(i)\, \log(P_{x+y}(i)) \tag{27}$$

$$\text{Difference Variance (DV)} = \text{var}\,iance\ of\ g_{x-y} \tag{28}$$

$$\text{Difference entropy (DE)} = -\sum_{i=0}^{G-1} P_{x+y}(i)\, \log(P_{x+y}(i)) \tag{29}$$

$$\text{Information measure of correlation1 (IMC1)} = \frac{HXY - HXY\ 1}{\max(HXHY)} \tag{30}$$

$$\text{Information measure of correlation 2 (IMC2)} = \sqrt{1-\exp\ [-2.0(HXY2 - HXY)]} \tag{31}$$

$$\text{Maximal Correlation Coefficient (MCC)} = (\text{second largest eigen value of Q})^{0.5} \tag{32}$$

$$\text{Inverse Difference Normalized (INN)} = \sum_{i,j}^{G} \frac{P_{ij}}{1+|i-j|^2 / G^2} \tag{33}$$

$$\text{Inverse different moment normalized (IDN)} = \sum_{i=0}^{G-1} \sum_{j=0}^{G-1} \frac{P_{(i,j)}}{1+|i-j|^2} \tag{34}$$

The extracted twenty two feature values from the predicted MFL images are listed in Table 1.

2.3. Artificial Neural Network Models

The entire 250 MFL Images are considered as a dataset. The total dataset is arbitrarily divided into two disjoint subsets, namely, training set containing 200 data (80 % of total dataset) and a test set comprising of 50 data (20 % of total dataset). The data simulated with different defect

Table 1. Twenty two GLCM Features extracted from the MFL images.

	GLCM Features extracted from the defects			
	Defect Dimension in mm Length/Depth/Width			
Feature Name	1/0.23/4.5	2/0.92/9	….	8/0.46/4.5
UNF	39.31701	12.77466	….	28.04681
ETR	1.196745	0.420188	….	0.549688
DSL	2.241101	2.800881	….	2.990163
CST	2.241101	2.800881	….	2.990163
ID	80.33101	324.3388	….	708.3407
CN	11.43705	29.67342	….	70.25436
H	0.74557	0.305676	….	0.483474
AC	1.088569	1.880914	….	1.092075
CS	5.185672	3.047913	….	5.064941
CP	2.932443	3.112431	….	3.018299
MP	2.919795	3.108349	….	3.014885
SS	1.666657	2.406602	….	1.535661
SA	39.45767	12.76967	….	28.01303
SV	22.22377	12.20957	….	17.98757
SE	102.3765	32.68507	….	67.75351
DV	4.571498	2.836458	….	4.670383
DE	1.196745	0.420188	….	0.549688
IMC(1)	1.856581	1.016194	….	1.405677
IMC(2)	-1.47162	-1.92439	….	-1.91998
MCC	2.522364	2.400993	….	2.772492
INN	3.171635	3.217211	….	3.196992
IDN	3.232901	3.243812	….	3.241661

dimensions such as length, width and depth are used in this work. Length ranging from 1 mm to 8 mm, depth ranging from 10 % to 60 % of total wall thickness and width ranging from 4.5 to 13.5 mm are considered.

The neural network models of feed-forward back propagation and cascade-forward back propagation are trained with the dataset of defect MFL Images. Different combinations of several internal parameters, *i.e.*, number of neurons, the number of hidden layers, transfer function, *etc.* are tried. Levenberg-Marquardt function produces better results, hence it was used as training function; Mean square error is a performance function used during training of feed-forward and cascade-forward back propagation neural network. There is no global method to determine the optimum values for the number of hidden layers, neurons in each hidden layer, *etc.* as they are functions of expected intelligence. For developing the NN models, neural network toolbox of Matlab R2014b software is used.

2.3.1. Feed-forward back propagation (FFBP) Model

The literature relating to neural network based defect characterization work is scarce. The existing literature is mostly devoted to the classification of the defect types. Very little work has been reported regarding sizing of defects. Neural network can be used to predict the defect shape and size from the MFL image [25]. The neural network is provided with both input and proper output (correct defect geometry) during the training phase. In the testing phase, NN is provided with only input. i.e. GLCM features extracted from the MFL image. Among the other network models, back propagation NN models are very popular though a large amount of data, and complex relationships between the different parameters exists. The FFBP neural network model consists of input, hidden and output layers. Total number of input nodes are 22, number of hidden layers are two, Number of neurons of the hidden layers are 16 and the number of output nodes are 3. The designed FFBP NN is shown in the Fig. 4.

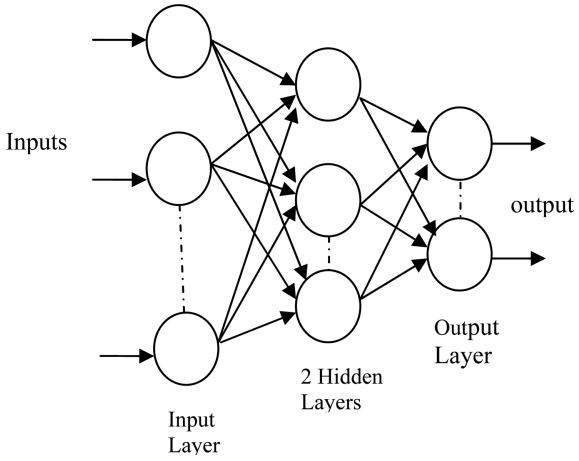

Fig. 4. Feed-forward back propagation model.

2.3.2. Cascade-forward back propagation Model

Cascade forward back propagation model shown in Fig. 5 is similar to feed-forward networks. In cascade forward back propagation networks, the first layer has weights coming from the input. Each succeeding layer has weights coming from the input and all previous layers. While two-layer FFBP networks can potentially learn any input output relationship, feed-forward networks with more layers might learn complex relationships more quickly. Compared to feed forward networks, a weight connection is included in CFBP models from input to each layer and from each layer to continual layers. The three layer network also has connections from the input to all three layers. The additional connections improve the speed at which the network learns the desired relationship. The performance of Cascade-forward back propagation and feed-forward back propagation is evaluated using MSE as given in eq. (35). It has

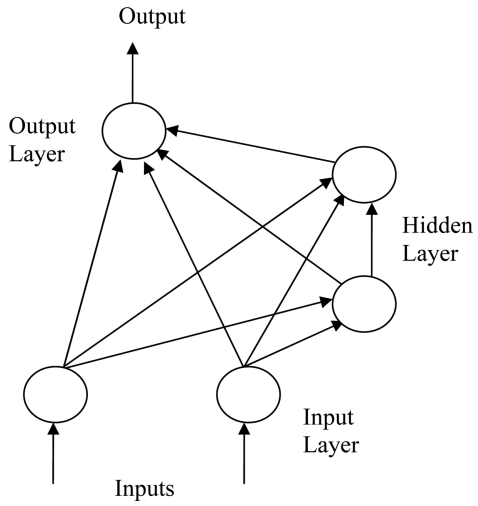

Fig. 5. Cascade-forward Back propagation model.

defined to minimise the training error. The model is designed with 22 numbers of input nodes, 2 hidden layers, 10 number of neurons and 3 number of output nodes.

$$MSE = \sum_{1}^{N} \left(\frac{Q_{\exp} - Q_{cal}}{n} \right)^2 \tag{35}$$

where,

$Q_{\exp}$ = Observed value
Q_{cal} = Predicted value
n = Number of observations in a dataset

Deciding the number of hidden layers and the number of neurons in the hidden layers is a very important part of deciding the overall neural network architecture. The better number will be achieved through trial and error basis. The number of neurons in each hidden layer varied from 1 to 17. Weights and biases are randomly initialized. The network is trained with maximum epochs reached. In this work, two artificial neural network models have been developed by applying cascade-forward and feed-forward back propagation techniques.

3. Results and Discussion

Magnetic Flux Leakage system for steam generator tube defect detection has been modeled using COMSOL 4.3a software. In the MFL inspection, the coil orientation is designed in such a way that the direction of magnetic flux is orthogonal to the defect. In this present work, MFL probe has been designed for detecting radial defect only. The outer surface radial defect is made on the 100 mm length steam generator tube with different dimensions such as length, depth and width. The defect features and its dimension ranges are depicted in Table 2. Modeled defect image that is obtained is noisy. Debauchies 4 wavelet denoising is applied. The surface plots of simulated noisy and filtered images are shown in Fig. 6.

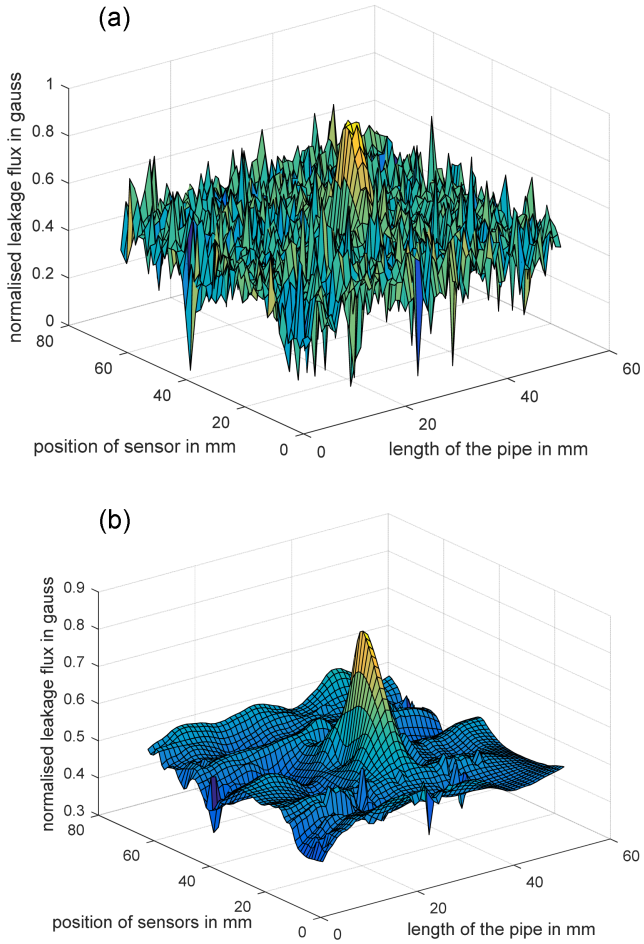

Fig. 6. (Color online) Surface Plot for (a) simulated noisy MFL image (b) denoised MFL image.

It is noted that the feature values shown in Table 1 are varying in relation to the change in any one or combination of defect dimensions. Fourteen haralick features in the GLCM represent the first order statistical characteristics and the remaining eight parameter represent the second order variant features with neibourhood pixel information. It clearly depicts the low and high frequency variation and the direction of propagation in the defect images, which help to identity edges. Hence all the features are taken as input to the neural network with actual defect

Table 2. Actual defect features and its dimension.

Defect	Dimension
Length	1 mm to 8 mm
Depth	10 % to 60 % of total wall thickness (2.3 mm)
Width	4.5 mm, 9 mm and 13.5 mm

Table 3. Results of defect characterization using Feed Forward Back propagation (FFBP) Network
l = length; d = depth; w = width in millimeter (mm).

True test data			Obtained test result			Error %		
L	D	W	L	D	W	L	D	W
1	0.69	13.5	1.058	0.672	13.19	–5.80	2.60	2.29
1	1.38	4.5	1.034	1.296	4.599	–3.40	6.08	–2.47
2	0.46	9	1.908	0.450	9.112	4.60	2.173	–1.240
2	0.92	13.5	2.110	0.902	13.69	–5.5	1.95	1.407
3	0.23	9	3.042	0.241	9.143	–1.40	–4.78	–1.588
3	1.15	4.5	3.046	1.190	4.408	–1.533	–3.47	2.040
4	0.69	9	3.962	0.681	9.286	0.950	1.304	–5.555
4	1.38	13.5	4.108	1.352	13.21	–2.70	2.020	2.148
5	0.46	4.5	4.909	0.446	4.320	1.820	3.043	4.000
5	1.15	13.5	5.104	1.192	13.21	–2.080	–3.65	2.148
6	0.92	4.5	5.902	0.909	4.385	1.633	1.195	2.555
6	0.23	9	6.225	0.219	9.199	–3.750	4.782	–2.211

Table 4. Results of defect characterization using Cascade Forward Back propagation (CFBP) Network.
l = length; d = depth; w = width in millimeter (mm)

True test data			Obtained test result			Error %		
L	D	W	L	D	W	L	D	W
1	0.69	13.5	1.112	0.652	13.01	–11.21	5.507	3.62
1	1.38	4.5	1.094	1.306	4.342	–9.40	5.36	3.51
2	0.46	9	2.181	0.421	9.265	–9.05	8.47	–2.94
2	0.92	13.5	2.095	0.949	13.21	–4.75	–3.15	2.14
3	0.23	9	3.162	0.211	9.287	–5.41	8.26	–3.18
3	1.15	4.5	3.089	1.221	4.372	–2.96	–6.17	2.84
4	0.69	9	3.769	0.653	9.461	5.77	5.36	–5.12
4	1.38	13.5	4.160	1.338	13.98	–4.00	3.04	–3.55
5	0.46	4.5	5.206	0.487	4.377	–4.12	–5.86	2.73
5	1.15	13.5	5.271	1.105	13.81	–5.42	3.91	–2.29
6	0.92	4.5	6.192	1.02165	4.301	–3.20	–10.97	4.42
6	0.23	9	6.243	0.250	9.291	–4.05	–8.69	–3.23

dimension (length, width and depth) as target.

The results of FFBP neural network and CFBP neural networks is evaluated in terms of charaterization accuracy and presented in Table 5 and Table 6. As the flaw in the pipe is non linear in nature, the tangent sigmoidal (tansig) as threshold function and Levenberg-Marquardt as learning algorithm are preferred for both the models.The CFBP model with two hidden layers having ten neurons in the layer produce the results with average percentage error of 5.77 %, 6.22 % and 3.29 % for length, depth and width respectively. For CFBP network the error does not back propagate to the input layer and conceives the forwarded input to the hidden layer. In FFBP network the error propogates to the input layer and trains the network parallaly. Hence the best results belong to FFBP model in terms of error accuracy and global convergence as shown in Fig. 7 and Fig. 8. A FFBP model with two hidden layers having

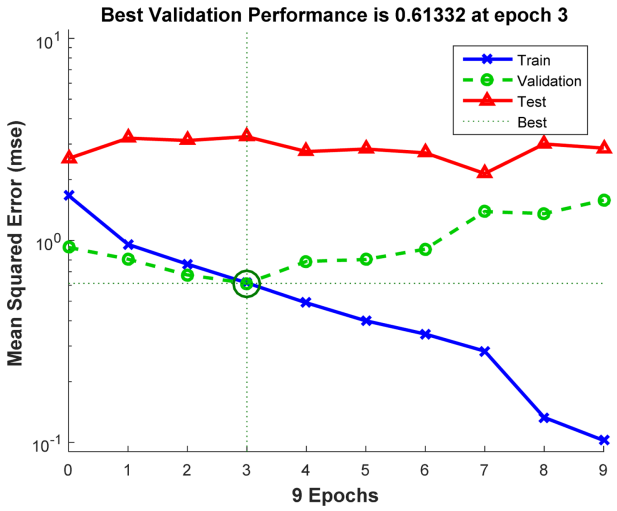

Fig. 7. (Color online) Performance plot of FFBP neural network.

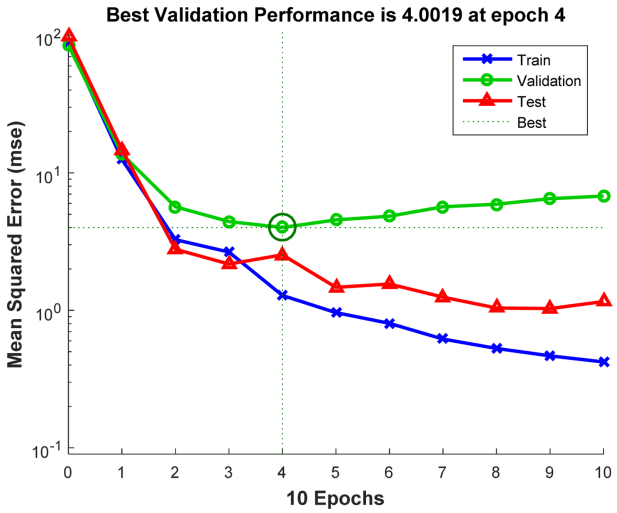

Fig. 8. (Color online) Performance plot of CFBP neural network.

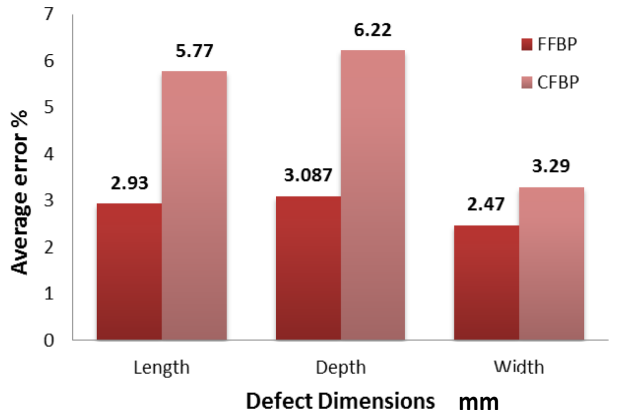

Fig. 9. (Color online) Percentage error of the two NN in defect characterization.

sixteen neurons for each layer gives the best results with average percentage error of 2.93 %, 3.087 % and 2.47 % for length, depth and width respectively.

The Actual defect volumes are calculated (length × depth × width). The percentage errors on volumetric defect are computed by comparing the predicted defect dimensions obtained by two neural network models with actual defect volumes. The percentage average error is plotted in Fig. 9. which shows the average error of length, depth and width of the defects obtained through FFBP and CFBP algorithms. FFBP algorithm produces smaller error percentage when compared to CFBP algorithms in characterizing the defects.

4. Conclusion

Neural network models based on feed-forward back propagation and cascade-forward back propagation algorithms are developed for the characterization of defects in MFL images. Gray level co-occurance features are extracted from defect images and given as input to the networks. The performances of the two developed neural network models are compared with MSE. Feed forward back propagation model exhibits best results (average length error of 2.93 %, average depth error of 3.087 % and average width error of 2.47 %) compared to cascade-forward back propagation model. feed-forward back propagation model with gray level co-occurance texture features provides an effective means for characterizing the defects in magnetic flux leakage images of steam generator tubes.

References

[1] Derac Son, Wonik Jung, Duck Gun Park, and Kwon Sang Ryu, IEEE Trans. Magn. **45**, 2724 (2009).
[2] P. Xiang, S. Ramakrishnan, X. Cali, P. Ramuhalli, R. Polikar, S. S. Udpa, and L. Udpa, Int. J. Appl. Electromagn. Mechan. **12**, 151 (2000).
[3] Baofu Lu, Belle and R. Upadhyaya, IEEE Trans. Nuclear Science **52**, 484 (2005).
[4] Ameet Joshi, Lalita Udpa, Satish Udpa, and Antonello Tamburrino, IEEE Trans. Magn. **42**, 3168 (2006).
[5] M. Li and D. A. Lowther, IEEE Trans. Magn. **46**, 3221 (2010).
[6] Maryam Ravan, Reza Khalaj Amineh, Slawomir Koziel, K. Natalia, Nikolova, and P. James, Reilly **46**, 1024 (2010).
[7] Yuji Gotoh and Norio Takahashi, IEEE Trans. Magn. **38**, 1209 (2002).
[8] Kenji Sakai, Koji Morita, YutaHaga, Toshihiko Kiwa, Katsumi Inoue, and Keiji T. Sukada, IEEE Trans. Magn. **51**, 11 (2015).
[9] J.-H. Kim, M.-H. Kim, and D.-H. Choi, J. Magn. **18**, 202 (2013).
[10] S. J. Farley, J. F. Durodola, N. A. Fellows, and L. H. Hernández-Gómez, NDT&E Int. **52**, 69 (2012).
[11] D.-G. Park, M. B. Kishore, J. Y. Kim, L. J. Jacobs, and D. H. Lee, J. Magn. **21**, 57 (2016).
[12] R. A. Chayjan, Australian J. Crop. Sci. **4**, 180 (2010).
[13] H. Demuth, M. Beale, and M. Hagan, Neural Network Toolbox User's Guide. The Mathworks, Inc., Natrick, USA (2009).
[14] D. S. Badde, A. K. Gupta, and K. V. Patki, IOSR J. Mech. and Civil Eng., 01-06.
[15] Sumit Goyal and Gyandera Kumar Goyal, Canadian Journal on Artificial Intelligence, Machine Learning and Pattern Recognition, **2** (2011).
[16] Francesco Riganti Fulginei and Alessandro Salvini, IEEE Trans. Magn. **48** (2012).
[17] A. A. Carvalho, J. M. A. Rebello, L. V. S. Sagrilo, C. S Camerini, and I. V. J. Miranda, NDT&E Int. **39**, 661 (2006).
[18] Debmalya Mukherjee, S. Saha, and S. Mukhopadhyay,

Inverse mapping of magnetic flux leakage signal for defect characterization, NDT&E Int. **54**, 198 (2013).
[19] Alaa Eleyan and Hasan Demirel. Co-occurrence matrix and its statistical features as a new approach for face recognition, Turk J. Elec. Eng. & Comp. Sci. **19**, 97 (2011).
[20] P. Karuppasamy, P. A. Abudhahir, M. Prabhakaran, S. Thirunavukkarasu, B. P. C. Rao, and T. Jayakumar, J. Non-destructive Evaluation **35**, 1 (2016).
[21] Yan Shi, Chao Zhang, Rui Li, Maolin Cai, and Guanwei Jia, Sensors **15**, 31036 (2015).
[22] Jackson Daniel, R. Mohanagayathri, and A. Abudhahir, IEEE International Conference on Electronics and Communication Systems (2014).
[23] A. David and Clausi, J. Can, Remote Sensing **28**, 45 (2002).
[24] Abdolvahab Ehsanirad and Y. H. Sharath Kumar, Oriental Journal of Computer Science & Technology **3**, 31 (2010).
[25] Mohamed Layouni, Sofiene Tahar, and Mohamed Salah Hamdi, IEEE Symposium on computational Intelligence for Engineering Solutions 14855753, 95 (2014).